Spectrochimica Acta Part A: Molecular and Biomolecular Spectroscopy 147 (2015) 107–116

Contents lists available at ScienceDirect

Spectrochimica Acta Part A: Molecular and Biomolecular Spectroscopy

journal homepage: www.elsevier.com/locate/saa

Synthesis, NMR, FT-IR, X-ray structural characterization, DFT analysis and isomerism aspects of 5-(2,6-dichlorobenzylidene)pyrimidine-2,4,6(1*H*,3*H*,5*H*)-trione

Assem Barakat [a,c,*,1], Hany J. Al-Najjar [a,1], Abdullah Mohammed Al-Majid [a,1], Saied M. Soliman [b,c,1], Yahia Nasser Mabkhot [a,1], Mohammed Rafi Shaik [a,1], Hazem A. Ghabbour [d,1], Hoong-Kun Fun [d,e,1]

[a] Department of Chemistry, College of Science, King Saud University, P.O. Box 2455, Riyadh 11451, Saudi Arabia
[b] Department of Chemistry, Rabigh College of Science and Art, King Abdulaziz University, P O Box 344, Rabigh 21911, Saudi Arabia
[c] Department of Chemistry, Faculty of Science, Alexandria University, P.O. Box 426, Ibrahimia, 21321 Alexandria, Egypt
[d] Department of Pharmaceutical Chemistry, College of Pharmacy, King Saud University, P.O. Box 2457, Riyadh 11451, Saudi Arabia
[e] X-ray Crystallography Unit, School of Physics, Universiti Sains Malaysia, Penang 11800, Malaysia

HIGHLIGHTS

- The 5-(2,6-dichlorobenzylidene)pyrimidine-2,4,6(1*H*,3*H*,5*H*)-trione was synthesized.
- The structure of **3** was determined using X-ray single crystal measurements.
- The calculated vibrational spectra are well correlated with the experimental data.
- Solvent effect on the electronic spectra of **3** was calculated by the TD-DFT method.
- The calculated NMR chemical shifts were well correlated with the experimental data.

GRAPHICAL ABSTRACT

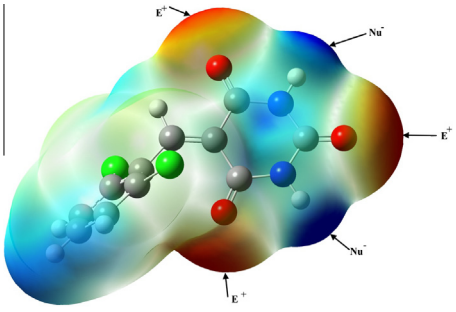

ARTICLE INFO

Article history:
Received 1 October 2014
Received in revised form 18 February 2015
Accepted 1 March 2015
Available online 19 March 2015

Keywords:
Pyrimidine
DFT
Isomers
NMR
Vibrational spectra

ABSTRACT

The synthesis and spectral characterization of the 5-(2,6-dichlorobenzylidene)pyrimidine-2,4,6(1*H*,3*H*,5*H*)-trione;**3** was reported. The solid state molecular structure of **3** was studied using X-ray crystallography. The relative stabilities of the seven possible isomers of **3** were calculated by DFT/B3LYP method using 6-311G(d,p) basis set. The calculated total energies and thermodynamic parameters were used to predict the relative stabilities of these isomers. The effect of solvent polarity on the relative stability of these isomers was studied at the same level of theory using PCM. It was found that the keto form, (T0), is the most stable isomer both in the gaseous state and solution. In solution, the calculated total energies of all isomers are decreased indicating that all isomers are stabilized by the solvent effect. The vibrational spectra of the most stable isomer, **3**(T0) are calculated using the same level of theory and the results are compared with the experimentally measured FTIR spectra. Good correlation was obtained between the experimental and calculated vibrational frequencies (R^2 = 0.9992). The electronic spectra of **3**(T0) in gas phase as well as in solutions were calculated using the TD-DFT method. All the predicted electronic transitions showed very little spectral shifts and increase in the intensity

* Corresponding author at: Department of Chemistry, College of Science, King Saud University, P.O. Box 2455, Riyadh 11451, Saudi Arabia. Tel.: +966 11467 5884; fax: +966 11467 5992.
E-mail address: ambarakat@ksu.edu.sa (A. Barakat).
[1] These authors contributed equally to this work.

http://dx.doi.org/10.1016/j.saa.2015.03.016

of absorption due to solvent effect. Also the ^{1}H- and ^{13}C-NMR chemical shifts of the stable isomer were calculated and the results were correlated with the experimental data. Good correlations between the experimental and calculated chemical shifts were obtained.

Introduction

The chemistry of the derivatives of barbituric acid, (pyrimidine-2,4,6(1*H*,3H,5*H*)-trione, which is the parent compound of barbiturates, has been a subject of permanent attention due to their significance in biology and medicine [1,2]. Thus, barbiturates are possessing pharmaceutical implementation in a variety of substances acting on the central nervous system. In addition to being used as anticonvulsants, anesthetics, and sedative hypnotics, most of them exert a hypnotic effect in larger doses and as sedative effect in small doses. Barbituric acid itself is not biologically active, and the pharmacological properties of barbituric acid mainly depends on the side groups attached to the C5 atom of the pyrimidine ring [1,2]. Recently, barbituric acid derivatives have also received great attention for nanoscience applications [3,4] besides being used extensively in therapy for many diseases. This is likely due to susceptibility to rapid metabolic attacked subsequent degradation of the compounds within the body, because of an acidic hydrogen at C-5 position [5,6]. 5-Benzylidene barbiturate derivatives have been shown to exhibit inhibitory effect against mushroom tyrosinase and antibacterial activities against Gram positive and Gram-negative bacteria [7]. Similarly, the related pyrimidine-trione derivatives are the key components of anticancer, HIV-1 and HIV-2 protease inhibitors, and anti-inflammatory drugs, such as veronal, seconal, bucolome, and sodium pentothal phenobarbital [8–15] (Fig. 1). Barakat et al. has reported an efficient method for the synthesis of a new series of barbituric acid scaffold and identified as NO free radicals scavenger [16]. In the light of the aforementioned facts, the present work aims to study the molecular structure, electronic and spectroscopic properties of the newly synthesized 5-(2,6-dichlorobenzylidene)pyrimidine-2,4,6(1*H*,3*H*,5*H*)-trione;**3**. The stability of the suggested seven isomers in the gas phase and in solution has been predicted using the total energies and thermodynamic parameters obtained from the DFT/B3LYP calculations. Also, the vibrational, electronic, and NMR spectra of the most stable isomer were predicted using the same level of theory.

Results and discussion

Chemistry

The synthetic strategy adopted to obtain the target compound was depicted in Scheme 1. The 5-(2,6-dichlorobenzylidene)pyrimidine-2,4,6(1*H*,3*H*,5*H*)-trione;**3** was synthesized by condensing the pyrimidine-2,4,6(1*H*,3*H*,5*H*)-trione;**1** with 2,6-dichlorobenzaldehyde **2** in the presence of aqueous diethylamine medium to yield the Aldol product.

The structure of the compound was determined by ^{1}H-NMR, ^{13}C-NMR, MS, IR, elemental analysis, and X-ray diffraction crystallography in a similar manner as those earlier compounds that were fully reported by our group [16].

X-ray diffraction

The structure of **3** (Fig. 2) was confirmed by X-ray crystal structure analysis. CCDC-1022573 contains the supplementary crystallographic data for this compound. These data can be obtained free of charge from the Cambridge Crystallographic Data Centre via www.ccdc.cam.ac.uk/data_request/cif.

A clear intense yellow block-like single crystal of $C_{11}H_6Cl_2N_2O_3$, of approximate dimensions 0.60 mm × 0.35 mm × 0.15 mm, was used for the X-ray crystallographic analysis. The frames were integrated with the Bruker SAINT software package using a narrow-frame algorithm [17,18]. The integration of the data using a triclinic unit cell, space group P-1, yielded a total of 30983 reflections to a maximum θ angle of 30.6 (0.70 Å resolution), of which 3624 were independent (completeness = 99.7%, R_{int} = 0.026). The final cell constants of a = 8.2291 (4)Å, b = 9.2702 (5)Å, c = 9.4942 (4)Å, α = 117.7620 (14)°, β = 94.4020 (13)°, γ = 106.9640 (13)°, volume = 593.35 (5)Å^3, are based upon the refinement of the *XYZ*-centroids of 3245 reflections above 20 $\sigma(I)$ with 5.0° < 2θ < 61.2°. Data were corrected for absorption effects using the multi-scan method (SADABS).

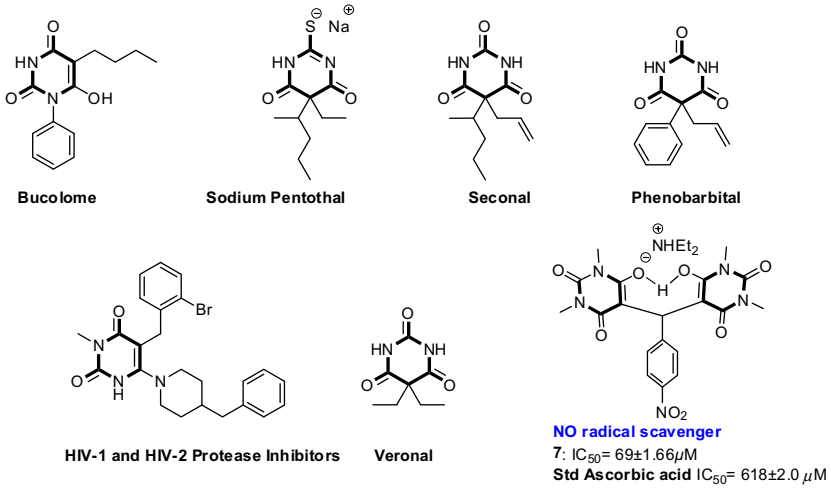

Fig. 1. Biologically active barbituric acid derivatives.

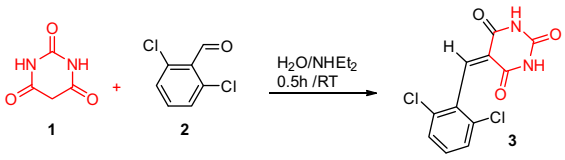

Scheme 1. Synthesis of 5-(2,6-dichlorobenzylidene)pyrimidine-2,4,6(1*H*,3*H*,5*H*)-trione;**3**.

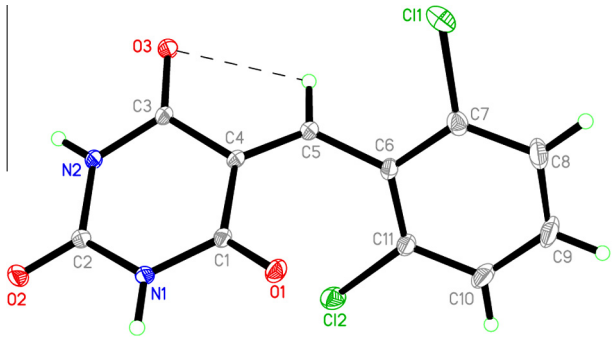

Fig. 2. ORTEP diagram of the compound **3** drawn at 50% ellipsoids for non-hydrogen atoms, showing the intramolecular hydrogen bond.

Table 1
Selected bond distances (Å) bond angles (°) and torsion angles (°) of compound **3**.

Cl1–C7	1.7375 (13)	N1–C1	1.3815 (15)
Cl2–C11	1.7364 (13)	N1–C2	1.3788 (17)
O1–C1	1.2161 (16)	N2–C2	1.3778 (17)
O2–C2	1.2175 (14)	N2–C3	1.3744 (15)
O3–C3	1.2188 (16)		
C1–N1–C2	125.71 (11)	O3–C3–C4	123.43 (10)
C2–N2–C3	126.05 (11)	N2–C3–C4	115.14 (11)
O1–C1–C4	124.05 (10)	O3–C3–N2	121.37 (11)
N1–C1–C4	114.93 (11)	Cl1–C7–C6	117.96 (9)
O1–C1–N1	121.01 (11)	Cl1–C7–C8	118.94 (10)
O2–C2–N1	121.98 (12)	Cl2–C11–C10	117.45 (10)
O2–C2–N2	121.52 (12)	Cl2–C11–C6	120.36 (9)
N1–C2–N2	116.49 (10)		
O1–N1–C1–C2	169.37 (10)	C4–C5–C6–C7	131.69 (13)
C2–N1–C2–C4	−9.95 (15)	C4–C5–C6–C11	55.58 (18)
C1–N1–C2–O2	177.40 (10)	C5–C6–C7–Cl1	177.61 (9)
C1–N1–C2–N2	−3.87 (15)	C7–C6–C11–Cl2	−175.91 (9)
C3–C4–C5–C6	−170.20 (10)	C9–C10–C11–C6	−.0.4 (2)

The asymmetric unit contains one moleclue of the compound. The molecular structure of compound **3** is composed of a pyrimidine ring (C1/N1/C2/N2/C3–C4) which is linked to a phenyl ring (C6–C11) through C5. The pyrimidine ring forms a dihedral angle of 47.87 (4)° with the adjacent benzene ring. The molecule is bent at the C5 atom with a C3–C4–C5–C6 torsion angle of −170.20 (10)° (Fig. 2). Selected bond distances (Å), bond angles (°) and torsion angles (°) of compound **3** are illustrated in Table 1. In the crystal structure, intermolecular C–H···O and N–H···O hydrogen bonds are observed (Fig. 3 and Table 2).

Computational details

All calculations for the studied isomers were carried out using Gaussian 03 software [19] on a Pentium IV processor personal computer. The calculations were performed by DFT/B3LYP method [20] using 6-311G(d,p) basis set [21]. The input file was taken from the CIF obtained from the X-ray single crystal measurements. The geometries were optimized by minimizing the energies with respect to all the geometrical parameters without imposing any molecular symmetry constraints. GaussView4.1 has been used to draw the structures of the optimized geometries [22]. The computational study was first carried out in gas phase, then, the Self-Consistent Reaction Field (SCRF) theory [23], with Polarized Continuum Model (PCM) was used [24] to predict the effect of solvent on the stability of the isomers studied [25]. Optimized structural parameters were used in the vibrational frequency, electronic property and isotropic chemical shift calculations. The electronic spectra of this compound were calculated by the TD-DFT method [26] in different solvents to predict the effect of solvent on the electronic spectra compared to the gas phase and for visualizing HOMO and LUMO states. The natural atomic charges are calculated using NBO calculations as implemented in the Gaussian 03 package

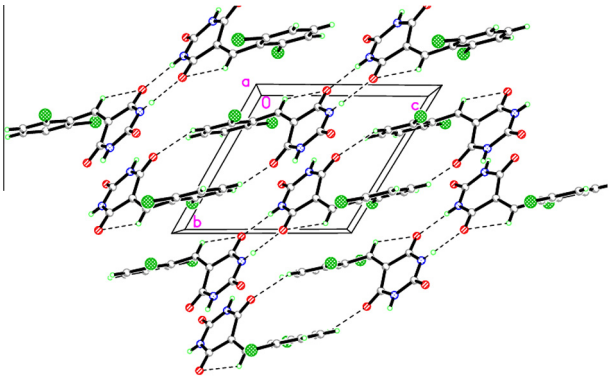

Fig. 3. Crystal packing showing intermolecular C–H···O and N–H···O hydrogen bonds as dashed lines.

Table 2
Hydrogen-bond geometry (Å, °).

D–H···*A*	*D*–H	H···*A*	*D*···*A*	*D*–H···*A*
N2–H1N2···O3^{i}	0.79 (2)	2.05 (2)	2.8342 (16)	176.2 (19)
N1–H1N1···O2^{ii}	0.858 (19)	2.058 (19)	2.8978 (15)	165.7 (17)
C5–H5A···O3	0.9300	2.4500	2.8121 (16)	103.00
C9–H9A···O2^{iii}	0.9300	2.5100	3.3897 (18)	157.00
C10–H10A···O1^{iv}	0.9300	2.5000	3.1748 (18)	130.00

Symmetry codes: (i) −*x* + 2, −*y*, −*z* + 1; (ii) −*x* + 3, −*y* + 1, −*z* + 1; (iii) *x* − 1, *y*, *z* − 1; (iv) −*x* + 2, −*y* + 1, −*z*.

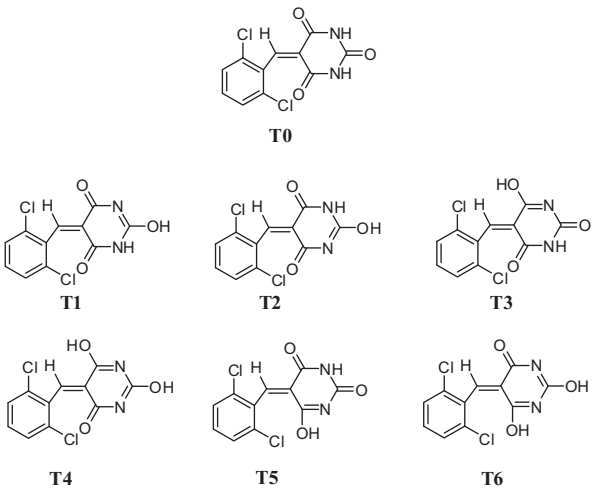

Scheme 2. The structure of the suggested possible isomers of the studied compound.

Table 3
Effect of solvent on the relative energies (ΔE, kcal/mol) of the studied isomers.

Isomer	ΔE[a]						
	T0	T1	T2	T3	T4	T5	T6
Ethanol	−20.17	−23.95	−23.83	−22.46	−24.46	−22.43	−24.52
Acetonitrile	−20.74	−11.15	−11.22	−23.09	−11.07	−23.11	−10.91
Chloroform	−14.61	−17.02	−16.96	−16.11	−17.31	−16.23	−17.49
Cyclohexane	−7.63	−8.71	−8.66	−8.27	−8.79	−8.37	−8.96

[a] $\Delta E = (E_{corr})_{solution} - (E_{corr})_{gas}$.

Table 4
Comparison between the calculated bond distances and bond angles of the most stable isomer (T0) of **3** with the experimental X-ray structure data.

Parameter[a]	DFT	X-ray	Parameter[a]	DFT	X-ray
R(1–15)	1.757	1.737	A(6-8-11)	114.6	114.9
R(2–22)	1.753	1.736	A(9-6-24)	115.4	116.9
R(3–8)	1.210	1.216	A(6-9-7)	114.2	116.5
R(4–9)	1.207	1.217	A(9-7-10)	127.9	126.0
R(5–10)	1.211	1.219	A(9-7-23)	115.5	117.9
R(6–8)	1.394	1.382	A(10-7-23)	116.6	116.0
R(6–9)	1.389	1.379	A(7-10-11)	115.0	115.1
R(6–24)	1.012	0.858	A(8-11-10)	120.0	118.4
R(7–9)	1.390	1.378	A(8-11-12)	123.4	123.5
R(7–10)	1.389	1.374	A(10-11-12)	116.6	118.0
R(7–23)	1.012	0.786	A(11-12-13)	114.9	116.0
R(8–11)	1.489	1.481	A(11-12-14)	129.2	128.1
R(10–11)	1.497	1.487	A(13-12-14)	115.9	116.0
R(11–12)	1.345	1.341	A(12-14-15)	119.4	119.5
R(12–13)	1.088	0.93	A(12-14-22)	123.9	124.2
R(12–14)	1.475	1.469	A(15-14-22)	116.6	116.0
R(14–15)	1.403	1.4	A(14-15-16)	122.6	123.1
R(14–22)	1.404	1.402	A(14-22-20)	121.8	122.1
R(15–16)	1.388	1.386	A(15-16-17)	119.8	120.6
R(16–17)	1.082	0.93	A(15-16-18)	118.9	118.8
R(16–18)	1.390	1.385	A(17-16-18)	121.3	120.6
R(18–19)	1.083	0.93	A(16-18-19)	119.8	119.8
R(18–20)	1.390	1.386	A(16-18-20)	120.4	120.4
R(20–21)	1.082	0.93	A(19-18-20)	119.8	119.8
R(20–22)	1.389	1.388	A(18-20-21)	120.9	120.2
A(1-15-14)	118.8	118.0	A(18-20-22)	119.7	119.6
A(1-15-16)	118.6	118.9	A(21-20-22)	119.4	120.2
A(2-22-14)	120.4	120.4	A(1-15-14)	118.8	118.0
A(2-22-20)	117.7	117.4	A(1-15-16)	118.6	118.9
A(3-8-6)	120.5	121.0	A(2-22-14)	120.4	120.4
A(3-8-11)	125.0	124.1	A(2-22-20)	117.7	117.4
A(4-9-6)	123.0	122.0	A(3-8-6)	120.5	121.0
A(4-9-7)	122.8	121.5	A(3-8-11)	125.0	124.1
A(5-10-7)	120.9	121.4	A(4-9-6)	123.0	122.0
A(5-10-11)	124.1	123.4	A(4-9-7)	122.8	121.5
A(8-6-9)	128.4	125.7	A(5-10-7)	120.9	121.4
A(8-6-24)	116.2	117.3	A(5-10-11)	124.1	123.4

[a] Atom numbering are referred to Fig. 3.

[27] at the DFT/B3LYP level. The nuclear magnetic resonance (NMR) chemical shifts calculations were performed using GIAO method [28,29] at the B3LYP level with 6-311G(d,p) basis set.

DFT calculations

Stabilities, relative energies and thermodynamic parameters of **3**

The studied molecule has three carbonyl and two NH groups so it can undergoes keto-enol as well as amine–imine tautomerization. Due to the presence of the exo-C=C bond, compound **3** can exhibit seven isomeric structures. The possible isomers of **3** are given in scheme 2. The total energies and thermodynamic parameters of these isomers are calculated using B3LYP/6-311G(d,p) method. The B3LYP/6-311G(d,p) calculated energies of the seven isomers are compared in Table S1 (Supplementary Materials) which shows that T0 has the lowest energy value (E = −1678.4821 Hartrees) among the studied isomers in the gas phase. This result was in good agreement with the experimentally measured X-ray structure of the studied compound. The relative abundances of the possible isomers were calculated using the equilibrium constants (K) calculated from the relation: $\Delta G = -RT\ln K$, where ΔG denotes the difference between the Gibbs free energies of a given isomer relative to the most stable one and K is the corresponding equilibrium constant. The abundance of the most stable species, T0 equal 100.0% at 298 K in the gas phase. The remaining species have zero total populations and are expected to be of no importance.

The stability of the studied isomers in different solvents were calculated using the polarized continuum model (PCM) at B3LYP/6-311G(d,p) level of theory. In solution the solute-solvent interactions between a given isomer and the solvent molecules could make significant changes in their relative stabilities. The calculated total energies and thermodynamic parameters of the different equilibrium reactions are given in Table S1 (Supplementary Materials). The effect of different solvents on the calculated relative energies (ΔE) is shown in Table 3. It could be noted that, the stability of all isomers increased in presence of solvent than in the gas phase where the more polar solvents such as ethanol and acetonitrile stabilize all the studied isomers more than the less polar solvents (cyclohexane and chloroform). However, the T0 isomer still the only form present in solution whatever the type of solvent used.

Molecular geometry

The optimized bond lengths and bond angles obtained for the stable isomer T0 using the B3LYP method with 6-311G(d,p) basis set are given in Table 4; while the atom numbering of the optimized structure is given in Fig. 4. The point group of the most stable isomer (T0) is C_1. The optimized geometrical parameters (bond distances and bond angles) and the experimental data obtained from the CIF are compared in Fig. 5. Most of the bond lengths are overestimated compared to the experimental data except the C=O bonds which are shorter than the experimental values. On the other hand, some of the bond angles are overestimated and others are underestimated. These deviations are attributed to the phase difference between the calculations and the experiment. The calculations refer to an isolated molecule in the gas phase, while the experimental data are those for the molecule in the solid phase. In general, the geometric parameters are predicted very well. The maximum deviations of the predicted bond length and bond angle values from the experimental data are 0.020 Å (C15–Cl1) and 2.654° (C8–N6–C9) respectively.

Natural atomic charges

The natural atomic charges (NAC) at the different atomic sites of the most stable isomer (T0) of **3** calculated using the DFT/B3LYP method were collected in Table 5. From the NAC values listed in Table 5, all the hydrogen atoms have positive charge densities within the range 0.2137–0.4250. The NH protons are the most electropositive H-atoms. The highest negative charge densities occur at the oxygen and nitrogen atoms as these sites are the most

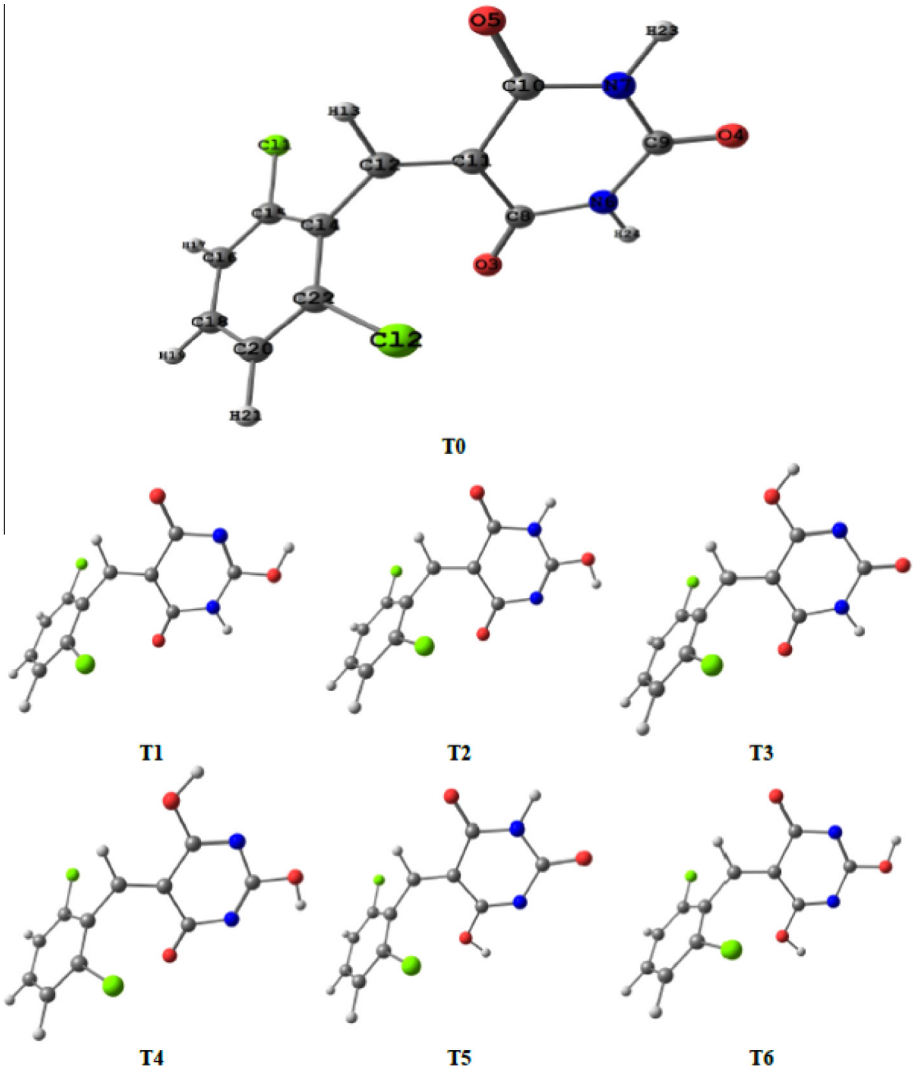

Fig. 4. The calculated optimized structures of the suggested isomers of the studied compound.

electronegative atoms in the studied molecule. Since the O-, N- and Cl-atoms are more electronegative than carbon so, all carbon atoms (C8, C9, C10, C15 and C22) bonded to the O-, N- and Cl-atoms are predicted to have positive charges. The most electropositive C-atom is C9 as it lies between one O- and two N-atoms. The rest of carbon atoms (C11, C12, C16, C18 and C20) have negative charge densities.

Molecular electrostatic potential (MEP)

The molecular electrostatic potential (MEP) was used for predicting site reactivity towards electrophilic and nucleophilic attack, and in studies of biological recognition and hydrogen bonding interactions [30,31]. The MEP of the stable isomer (T0) of **3** calculated using B3LYP with 6-311G(d,p) basis set was used to predict the reactive sites for electrophilic and nucleophilic attack. The negative (red) regions of the MEP are related to electrophilic reactivity and the positive (blue) regions to nucleophilic reactivity, as shown in Fig. 6. As can be seen from this figure, negative regions are mainly localized over the carbonyl oxygen atoms (−0.0391 to −0.0415 au) while the maximum positive regions are localized on the hydrogen atoms (0.0447 to 0.0480 au) of the NH groups. Hence, it would be predicted that the carbonyl oxygen atoms and the amine hydrogen of the amide groups are the most reactive sites for electrophilic and nucleophilic attack respectively [32]. These sites give information about the region from where the compound can make intermolecular H-bonding interactions.

Analysis of the vibrational spectra

The infrared vibrational frequencies of the most stable isomer of the titled compound were calculated using the DFT B3LYP/6-311G(d,p) method. The calculated and the experimental infrared vibrational frequencies and intensities are given in Table S2 (Supplementary Information). Selected calculated vibrational frequencies are compared with the experimental vibrational frequencies (see Table 6). Vibrational mode assignments were made by the visual inspection of the modes animated by using GaussView program [22] and the results were presented in Table 6. The experimental and predicted IR spectra of the titled compound were given in Fig. 7. The scaled infrared vibrational frequencies showed good agreement with the experimental data. A correlation graph between the calculated and the experimental vibrational frequencies is shown in Fig. 8. As can be seen from this figure, good correlation was obtained between the calculated and the experimental vibrational frequencies with high correlation coefficient (R^2 = 0.9992).

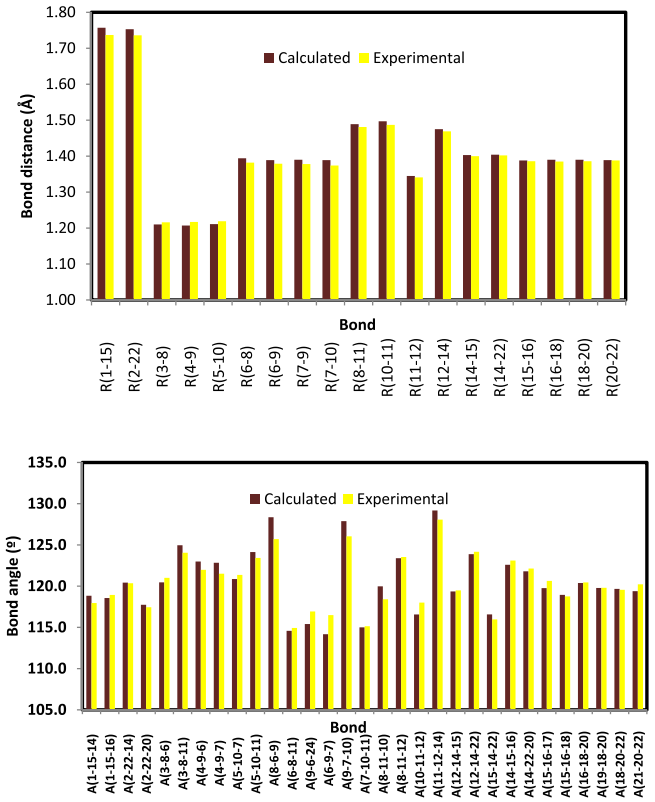

Fig. 5. Comparison between the calculated and experimental geometric parameters of the studied compound.

N–H vibrations

The ν_{NH} stretching vibration of the secondary amines appeared around 3500–3000 cm^{-1} in the IR absorption spectra [34]. The weak band appeared experimentally at 3459 cm^{-1} (calc. 3483–3481 cm^{-1}) is due to N–H stretching vibrations. Also the in-plane N–H bending vibrations of the amine groups appeared at 1379 and 1350 cm^{-1} (calc. 1382–1357 cm^{-1}) while the out-of-plane bending modes appeared in the range of 686–613 cm^{-1} (calc. 667–610 cm^{-1}).

C–H vibrations

The three aromatic C–H stretching vibrations of **3** are calculated at 3108, 3103 and 3081 cm^{-1} which occur in the characteristic region of the aromatic C–H stretching vibrations [34]. In the present investigation, the IR bands identified experimentally for the C–H stretching vibrations at 3017 and 2971 cm^{-1}. The latter is calculated at lower frequency (calc. 3037 cm^{-1}) than the aromatic C–H stretching vibration and assigned for the $\nu_{(=C-H)}$ of the methylene group.

The bands corresponding to the in-plane and out-of-plane ring C–H deformations are observed in the region 1400–1000 and 1000–600 cm^{-1} [33,35], respectively. In the present study, the DFT calculations predicted the C–H in-plane bending modes of **3** at 1420, 1275, 1179 and 1166 cm^{-1} while the out-of-plane C–H deformations were predicted at 955, 760 and 754 cm^{-1}. These results were in good agreement with the experimentally observed data (Table 6).

C=O vibrations

The studied molecule has three C=O groups so, three $\nu_{C=O}$ are predicted. The stretching vibrations of the C=O bonds are calculated using the B3LYP calculations at 1769, 1743 and 1711 cm^{-1}. The former band was observed at 1738 cm^{-1} which is assigned to the stretching vibration of the C9=O4. The two vibrational bands (calc. 1743 and 1711 cm^{-1}) are due to the symmetric and asymmetric stretching vibrations of the other two carbonyls groups, respectively. The lower frequency of these $\nu_{C=O}$ vibrations than expected is due to the conjugation effect with the arylidene ring.

C=C vibrations

The ring C=C stretching vibrations occur in the region of 1625–1400 cm^{-1} [36]. Almost the C=C stretching vibrations are found overlapped with other vibrations and difficult to be assigned. The present DFT calculations predicted the C=C stretching vibrations of **3** at 1613, 1569 and 1541 cm^{-1}. These stretching vibrations are observed experimentally at 1614, 1555 and 1490 cm^{-1}, respectively.

Frontier molecular orbitals (FMOs) and electronic absorption spectra

The frontier molecular orbitals (HOMO and LUMO) are important quantum chemical parameters used to describe the molecular reactivity and the ability of a molecule to electron transport. The orbital energy level analysis of studied compound showed that E_{HOMO} and E_{LUMO} values are −7.2995 and −3.0126 eV, respectively. The energies of HOMO and LUMO are negative, which indicates that the studied molecule is stable [37].The HOMO–LUMO energy gap represents the lowest energy electronic transition. The HOMO–LUMO energy gap of **3** calculated at the DFT level is 4.2869 eV. The HOMO and LUMO plots drawn by DFT-B3LYP method is shown in Fig. 9. The HOMO level of is mainly localized on the aryl group while LUMO is populated on the whole π-system

Table 5
The calculated natural atomic charge densities of the most stable isomer (T0) of **3**.

Atom	NAC	Atom	NAC
Cl1	0.0142	H13	0.2431
Cl2	0.0146	C14	−0.1395
O3	−0.5649	C15	0.0203
O4	−0.5871	C16	−0.2259
O5	−0.5797	H17	0.2247
N6	−0.6513	C18	−0.1579
N7	−0.6506	H19	0.2137
C8	0.6794	C20	−0.2220
C9	0.8298	H21	0.2245
C10	0.6881	C22	0.0299
C11	−0.2335	H23	0.4250
C12	−0.0197	H24	0.4247

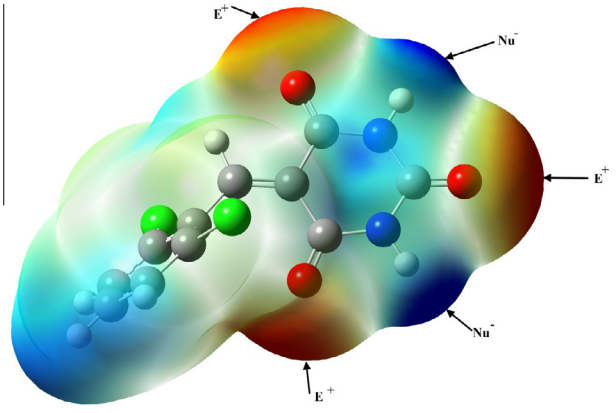

Fig. 6. Molecular electrostatic potentials (MEP) mapped on the electron density surface calculated by the DFT/B3LYP method for the stable isomer (T0) of **3**.

Table 6
The calculated and experimental wavenumbers of the most stable isomer (T0) of **3**.

Assignment	Calculated	Experimental
ν_{NH}	3483, 3481	3459
$\nu_{(CH,\ aromatic)}$	3108, 3103, 3081	3017
$\nu_{(=CH)}$	3037	2971
$\nu_{(C9=O4)}$	1769	1738
$\nu_{(C8=O3+C10=O5)sym}$	1743	
$\nu_{(C8=O3+C10=O5)assym}$	1711	1683
$\nu_{C=C}$	1613, 1569, 1541	1614, 1555, 1490
$\delta_{CH\ in\ plane}$	1420, 1275, 1179, 1166	1438, 1282, 1205, 1167
$\delta_{NH\ in\ plane}$	1382, 1357	1379, 1350
$\delta_{CH\ out\ plane}$	955, 760, 754	998, 765, 736
$\delta_{NH\ out\ plane}$	667, 610	686, 613

υ: streching , δ: bending.

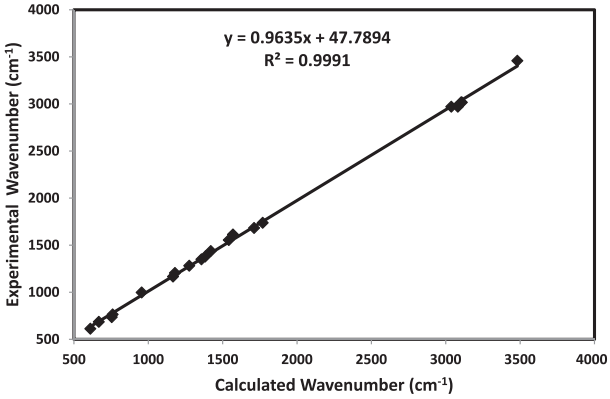

Fig. 8. correlation graph between the calculated and experimental vibrational frequencies of the isomer (T0) of **3**.

of the studied molecule. Hence, the HOMO → LUMO electronic transition is mainly belongs to $\pi \rightarrow \pi^*$ transition.

The possible electronic transitions in the UV–Visible spectrum of **3** have been studied by the time-dependent density functional theory (TD-DFT). The first twenty spin allowed singlet-singlet excitations were calculated using TD-DFT calculations in the gas phase as well as in solutions of different polarity solvents. The calculated electronic transitions of high oscillatory strength are given in Table 7. Theoretical UV–Visible spectrum of the compound is shown in Fig. 10 and Fig. S1 (Supplementary Information). The six most intense spectral bands are calculated at 199.6, 218.4, 244.9, 273.6, 333.6 and 361.9 nm in the gas phase. The major contributions of molecular orbitals involved in these transitions are shown in Table 7. For example, the longest wavelength transition band (361.9 nm) corresponds to the electronic transition from the H, H-1 and H-2 to LUMO with 37%, 33% and 24% contributions, respectively. The experimental electronic spectra of the studied compound in different solvents are given in Fig. S2 (Supplementary Information). Experimentally, we observed two

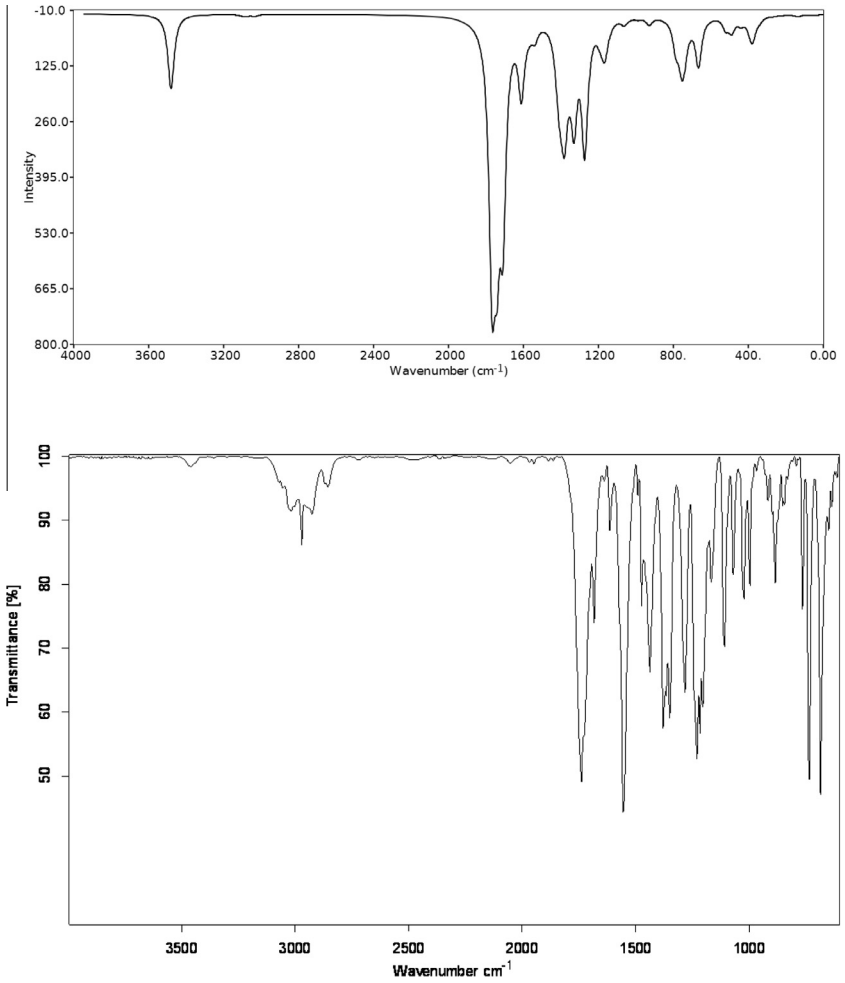

Fig. 7. The experimental (lower) and calculated scaled (upper) infrared vibrational spectra of the studied compound.

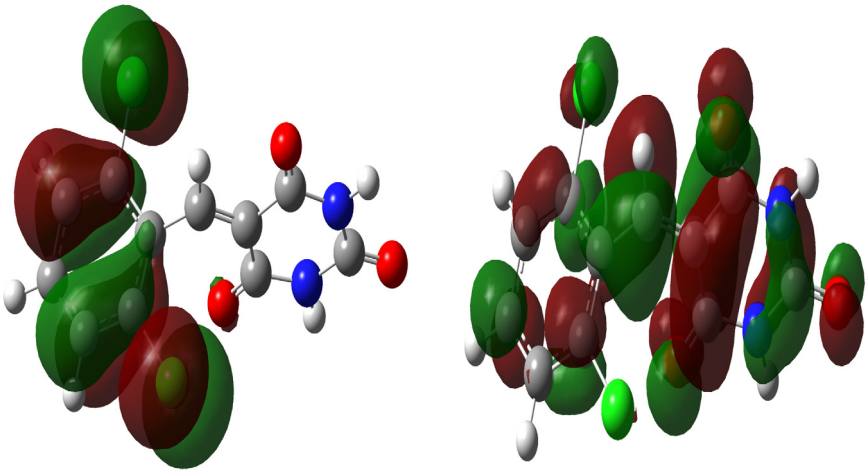

Fig. 9. The ground state isodensity surface plots of the frontier molecular orbitals of the studied molecule.

Table 7
The calculated electronic transitions of the most stable isomer (T0) of **3** using the TD-DFT method.

Solvent	λ_{max}	f_{osc}	Major contribution
Gas	361.9	0.023	H-2 → L (24%), H-1 → L (33%), H → L (37%)
	333.6	0.072	H-2 → L (57%), H-1 → L (34%)
	273.6	0.043	H-6 → L (57%), H-4 → L (22%)
	244.9	0.141	H-8 → L (20%), H-6 → L (24%), H-5 → L (22%), H-4 → L (17%)
	218.4	0.095	H-9 → L (10%), H-1 → L + 2 (22%), H → L + 1 (30%)
	199.6	0.280	H-2 → L + 1 (19%), H-1 → L + 1 (19%), H → L + 2 (20%)
Cyclohexane	361.8	0.040	H-2 → L (15%), H-1 → L (39%), H → L (41%)
	334.7	0.064	H-2 → L (73%), H-1 → L (20%)
	271.8	0.052	H-6 → L (64%), H-4 → L (15%)
	245.9	0.230	H-8 → L(13%), H-6 → L(19%), H-5 → L (31%), H-4 → L (10%), H-3 → L (14%)
	218.8	0.104	H-1 → L + 2 (23%), H → L + 1 (42%)
	200.8	0.403	H-2 → L + 1 (34%), H-1 → L + 1 (17%), H → L + 2 (19%)
Chloroform	361.1	0.047	H-2 → L (14%), H-1 → L (38%), H → L (43%)
	333.8	0.063	H-2 → L (76%), H-1 → L (17%)
	271.6	0.061	H-6 → L (59%), H-3 → L (25%)
	245.6	0.232	H-8 → L (12%), H-6 → L (22%), H-5 → L (32%), H-3 → L (12%)
	218.3	0.089	H-1 → L + 2 (25%), H → L + 1 (43%)
	200.3	0.366	H-2 → L + 1 (35%), H-1 → L + 1 (16%), H → L + 2 (19%)
Acetonitrile	359.4	0.048	H-2 → L (13%), H-1 → L (39%), H → L (43%)
	332.2	0.056	H-2 → L (77%), H-1 → L (15%)
	270.7	0.062	H-6 → L (55%), H-3 → L (27%)
	244.5	0.231	H-8 → L (11%), H-6 → L (22%), H-5 → L (33%), H-4 → L (13%)
	217.7	0.076	H-1 → L + 2 (26%), H → L + 1 (41%)
	199.5	0.303	H-2 → L + 1 (30%), H-1 → L + 1 (16%), H → L + 2 (18%)
Ethanol	359.8	0.051	H-2 → L (14%), H-1 → L (35%), H → L (46%)
	332.7	0.066	H-2 → L (75%), H-1 → L (17%)
	271.4	0.065	H-6 → L (54%), H-3 → L (25%)
	244.9	0.220	H-8 → L (12%), H-6 → L (24%), H-5 → L (35%), H-4 → L (11%)
	217.7	0.079	H-1 → L + 2 (25%), H → L + 1 (42%)
	199.8	0.335	H-2 → L + 1 (32%), H-1 → L + 1 (16%), H → L + 2 (19%)

intense transition bands around 202 nm (calc. ~200 nm) and 222 nm (calc. ~218 nm). It can be seen from Fig. 9 that, the calculated absorption wavelengths showed little variations in all the studied solvents compared to the gas phase. It is noted that, the absorption intensities of all the spectral bands are higher in presence of solvent compared to the gas phase. In agreement with the calculations, the experimental electronic spectra showed also little variations due to solvent effects.

Nonlinear optical (NLO) effects

NLO is very important in areas such as optical interconnections, telecommunications and signal processing [38,39]. Polarizability (α) is important electronic parameter in the discussions of the NLO of a molecule. The average polarizability (α_0) of the studied compound is compared to urea which is used as a reference molecule [40]. The α_0 of the studied compound and urea are calculated to be 163.92 and 28.00 au, respectively. The polarizability of the title compound is about 6 times greater than urea. Thus, **3** could be a better NLO material compared to urea. Moreover, good nonlinear optical properties materials are molecules having small to moderate excitation energies so, the nonlinear optical properties are related to the energy gap between HOMO and LUMO where the small HOMO–LUMO gap (ΔE) requires small excitation energy [41,42]. The energy gap (ΔE) for the studied molecule is calculated

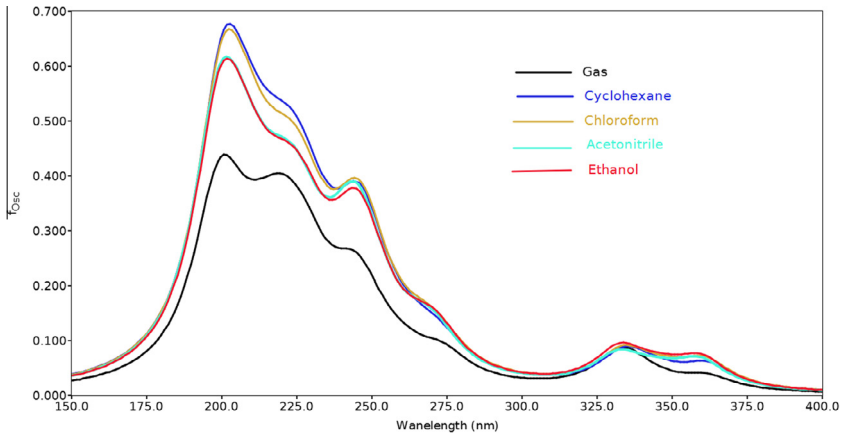

Fig. 10. The calculated electronic spectra of the most stable isomer (T0) of **3** in gas phase and in solution using TD-DFT method.

Table 8
The experimental and GIAO calculated chemical shift values of the studied compound using DFT/B3LYP.

Atom	$(CS)_{calc.}$	$(CS)_{Exp.}$
C8	162.1	162.3
C9	150.0	150.7
C10	163.1	162.3
C11	127.5	125.2
C12	162.7	161.0
C14	140.5	133.7
C15	147.4	147.8
C16	132.9	132.5
C18	134.8	128.4
C20	133.5	131.2
C22	149.4	147.8
H13	8.44	8.13
H17	7.26	7.52
H19	7.25	7.43
H21	7.31	7.52
H23	6.49	11.61
H24	6.32	11.38

to be 4.2869 eV which is lower than urea (7.6644 eV). These results indicated that the studied compound has better NLO properties than urea.

NMR spectra

The isotropic magnetic shielding (IMS) values calculated using the GIAO approach at the 6-311G(d,p) level are used to predict the ^{13}C and ^{1}H chemical shifts (δ_{calc}) for the T0 isomer. The experimental and theoretical chemical shift values of the T0 isomer are given in Table 8. The theoretical ^{1}H and ^{13}C NMR chemical shifts of the **3**(T0) have been compared with the experimental data (ΔE_{xp}). According to these results, the calculated chemical shifts are in accord with the experimental findings. The correlation graphs between the experimental and calculated chemical shifts are shown in Fig. 11. The correlation graphs follow the linear equations. The correlation coefficients (R^2) of the ^{1}H-NMR and ^{13}C-NMR are 0.5059 and 0.9740, respectively showing that there is better agreement between the experimental and calculated chemical shifts for carbons than protons. The protons located at terminal positions in the molecule and more subjected to interaction with solvent molecules. We noted that, the δ_{calc} of the NH protons strongly deviate from the experimental data due to the high polarity of these bonds. These polar bonds interact strongly with the solvent molecules. From this point of view, the chemical shift values of these protons are omitted from the correlation and better correlation coefficient is obtained (R^2 = 0.9886).

Experimental section

General remarks

All the chemicals were purchased from Sigma–Aldrich, Flukaetc, and were used without further purification, unless otherwise stated. Melting point was measured on a Gallenkamp melting point apparatus in open glass capillaries and is uncorrected. IR Spectra were measured as KBr pellets on a Nicolet 6700 FT-IR spectrophotometer. The NMR spectra were recorded on a Jeol-400 NMR spectrometer. ^{1}H-NMR (400 MHz), and ^{13}C-NMR (100 MHz) were run in deuterated chloroform ($CDCl_3$). Chemical shifts (δ) are referred

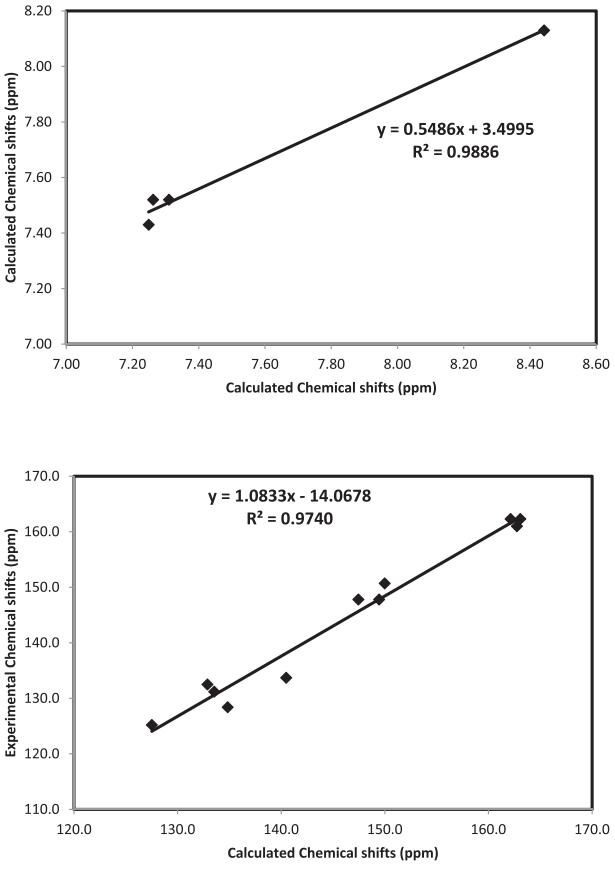

Fig. 11. The correlation graph between the ^{1}H-NMR (upper) and ^{13}C-NMR (lower) calculated chemical shifts and the experimental data. *Note:* The δ_{calc} of H23 and H24 are omitted from the correlation graphs.

in terms of *ppm* and *J*-coupling constants are given in *Hz*. Mass spectra were recorded on a Jeol of JMS-600 H. Elemental analysis was carried out on Elmer 2400 Elemental Analyzer; CHN mode.

*Synthesis of 5-(2,6-dichlorobenzylidene)pyrimidine-2,4,6(1H,3H,5H)-trione (**3**)*

A mixture of 2,6-dichlorobenzaldehyde **2**(3 mmol, 525 mg), pyrimidine-2,4,6(1*H*,3*H*,5*H*)-trione;**1** (6 mmol, 384 mg), and diethylamine (3 mmol, 310 μl) in 3 mL of degassed H_2O was stirred at room temperature for 0.5hour, the crude product was extracted with mixture of DCM/EtOH, was with 10% HCl (2 * 10 mL), the organic phase was with brine and recrystallized from DCM/EtOH to afford **3** yellow crystalline material (0.77 g, 2.7 mmol, 90%). m.p: 208 °C; IR (KBr, cm^{-1}): 3459, 3017, 2971, 1738, 1683, 1614; ^{1}H-NMR (400 MHz, DMSO-d_6): δ11.61 (bs, 1H, NH), 11.38 (bs, 1H, NH), 8.13(s, 1H, CH═), 7.52(d, 2H, *J* = 8.0 Hz, Ph), 7.43 (t, 1H, *J* = 8.0 Hz, Ph);^{13}C-NMR (100 MHz, DMSO-d_6): δ = 162.3, 161.0, 150.7, 147.8, 133.7, 132.5, 131.2, 128.4, 125.2; LC/MS (ESI): 283.98 $[M]^+$; Anal. for $C_{11}H_6Cl_2N_2O_3$; calcd: C, 46.34; H, 2.12; Cl, 24.87; N, 9.83; Found: C, 46.34; H, 2.12; Cl, 24.87; N, 9.83.

Conclusions

The 5-(2,6-dichlorobenzylidene)pyrimidine-2,4,6(1*H*,3*H*,5*H*)-trione;**3** was synthesized and characterized using elemental analyses, FTIR, ^{1}H- and ^{13}C-NMR spectra. Single crystal X-ray structure determination showed its 3D structure and its packing in the crystalline state. The stability and populations of the seven suggested isomers of **3** were predicted using the DFT/B3LYP method. The effect of solvent on their relative stability was studied using polarized continuum model (PCM). All isomers are more or less stabilized in presence of solvent effect compared to the gas phase. The DFT calculations confirmed that the trione is the only form of **3** that could exist either in the gas phase or in solution. The spectroscopic and electronic properties of the studied compound were calculated using the same level of theory. The calculated infrared vibrational frequencies of the fundamental modes showed good correlations with the experimental data. The electronic spectra in the gas phase and in solution of different solvents are very similar, with the exception that there is an increase in the intensity of the absorption which were noted in solution. The electronic properties such as polarizability and HOMO–LUMO energy gap predicted higher NLO activity of **3** compared to urea. MEP study showed that the O-atoms and the NH protons are the most reactive sites towards electrophilic and nucleophilic attack respectively.

Conflicts of interest

The authors declare no conflict of interest.

Acknowledgments

The authors would like to extend their sincere appreciation to the Deanship of Scientific Research at King Saud University for its funding this Research group NO (RG -257-1435-1436).

Appendix A. Supplementary data

Supplementary data associated with this article can be found, in the online version, at http://dx.doi.org/10.1016/j.saa.2015.03.016.

References

[1] J.T. Bojarski, J.L. Mokrosz, H.J. Barton, M.H. Paluchowska, in: A.R. Katritzky (Ed.), Recent Progress in Barbituric Acid Chemistry in Advances in Heterocyclic Chemistry, vol. 38, Academic Press Inc, New York, 1985, references therein.
[2] G.L. Patrick, An Introduction to Medicinal Chemistry, fourth ed., Oxford University Press, Oxford, 2009. p. 752.
[3] D.M. Bassani, Chimia 60 (2006) 175–178.
[4] A. Ikeda, Y. Tanaka, K. Nobusawa, J.-I. Kikuchi, Langmuir 23 (2007) 10913–10915.
[5] W.O. Foy, T.L. Lemke, D.A. Williams, Principles of Medicinal Chemistry, fourth ed., Williams and Wilkins, 1995. p. 385.
[6] L.S. Goodman, A. Gilman, The Pharmacological Basis of Therapeutics, fourth ed., Macmillan, New York, 1970. p. 98 (Chapter 9).
[7] Q. Yan, R. Cao, W. Yi, Z. Chen, H. Wen, L. Ma, H. Song, Eur. J. Med. Chem. 44 (2009) 4235–4243.
[8] L.S. Goodman, A. Gilman, The Pharmacological Basis of Therapeutics, McGraw-Hill, New Delhi, 1991. pp. 358–360.
[9] G. Andrews, Medical Pharmacology, The CV Mosby Co., Saint Louis, MO, 1976. pp. 243–250.
[10] W.O. Foye, Principles of Medicinal Chemistry, Lea & Febiger, Pennsylvania, PA, 1989. pp. 143–237.
[11] D.J. Guerin, D. Mazeas, M.S. Musale, F.N.M. Naguib, O.N.A. Safarjalani, M.H. Kouni, R.P. Panzica, Bioorg. Med. Chem. Lett. 9 (1999) 1477–1480.
[12] E. Fisher, J.R. Moring, Ther. Ggw. 44 (1903) 97–105.
[13] W.J. Doran, Med. Chem. 4 (1959) 164–167.
[14] B. Bobranski, Wiad. Chem. 31 (1977) 231–278.
[15] S. Senda, H. Izumi, H. Fujimura, Arznein. Forsch. 17 (1967) 1519–1523.
[16] A. Barakat, A.M. Al-Majid, H.J. Al-Najjar, Y.N. Mabkhot, S. Yousuf, M.I. Choudhary, Eur. J. Med. Chem. 84 (2014) 146–154.
[17] Bruker, APEX2, SAINT and SADABS. Bruker AXS Inc., Madison, Winconsin, USA, 2009.
[18] G.M. Sheldrick, A short history of SHELX, Acta Crystallogr. A64 (2008) 112–122.
[19] M.J. Frisch et al., Gaussian-03, Revision C.01, Gaussian Inc, Wallingford, 2004.
[20] P. Hohenberg, W. Kohn, Phys. Rev. 136 (1964) B864.
[21] (a) A.D. McLean, G.S. Chendler, J. Chem. Phys. 72 (1980) 5639–5648; (b) R. Krishnan, J.S. Binkley, R. Seeger, J.A. Pople, J. Chem. Phys. 72 (1980) 650–654.
[22] GaussView, Version 4.1, R. Dennington II, T. Keith, J. Millam, Semichem Inc., Shawnee Mission, KS, 2007.
[23] A.D. Becke, Phys. Rev. A 38 (1988) 3098–3100.
[24] (a) M.T. Cancès, B. Mennucci, J. Tomasi, J. Chem. Phys. 107 (1997) 3032–3041; (b) M. Cossi, V. Barone, B. Mennucci, J. Tomasi, Chem. Phys. Lett. 286 (1998) 253–260; (c) B. Mennucci, J. Tomasi, J. Chem. Phys. 106 (1997) 5151–5158; (d) M. Cossi, G. Scalmani, N. Rega, V. Barone, J. Chem. Phys. 117 (2002) 43–54.
[25] W. Wang, W.J. Mortier, J. Am. Chem. Soc. 108 (1986) 5708.
[26] (a) R.E. Stratmann, G.E. Scuseria, M.J. Frisch, J. Chem. Phys. 109 (1998) 8218–8224; (b) R. Bauernschmitt, R. Ahlrichs, Chem. Phys. Lett. 256 (1996) 454–464; (c) M.E. Casida, C. Jamorski, K.C. Casida, D.R. Salahub, J. Chem. Phys. 108 (1998) 4439–4449.
[27] E.D. Glendening, A.E. Reed, J.E. Carpenter, F. Weinhold, NBO Version 3.1, CI, University of Wisconsin, Madison, (1998).
[28] A.E. Reed, L.A.F. Curtiss, Chem. Rev. 88 (1988) 899.
[29] M.J. Frisch, J.A. Pople, J.S. Binkley, J. Chem. Phys. 80 (1984) 3265.
[30] J.S. Murray, K. Sen, Molecular Electrostatic Potentials, Concepts and Applications, Elsevier, Amsterdam, 1996.
[31] (a) E. Scrocco, J. Tomasi, Adv. Quantum Chem. 11 (1978) 115–196; (b) M. Ramegowda, New J. Chem. 37 (2013) 2648–2653; (c) M. Zhang, B. Ren, Y. Wang, C. Zhao, Spectrochim. Acta Part A 101 (2013) 191–195.
[32] B. Galabov, D. Cheshmedzhieva, S. Ilieva, B. Hadjieva, J. Phys. Chem. A 108 (51) (2004) 11457–11462.
[33] G. Socrates, Infrared and Raman Characteristic Group Frequencies, Tables and Charts, third ed., Wiley, Chichester, 2001.
[34] G. Varsanyi, Vibrational Spectra of 700 Benzene Derivatives, vols. (I–II) AkademicKiego, Budapest, 1974.
[35] G. Varsanyi, Vibrational Spectra of Benzene Derivatives, Academic Press, New York, 1969.
[36] V. Krishnakumar, N. Surumbarkuzhali, S. Muthunatesan, Spectrochim. Acta Part A 71 (2009) 1810–1813.
[37] S.W. Xia, X. Xu, Y.L. Sun, Y.L. Fan, Y.H. Fan, C.F. Bi, D.M. Zhang, L.R. Yang, Chin. J. Struct. Chem. 25 (2006) 849–853.
[38] V.M. Geskin, C. Lambert, J.L. Bredas, J. Am. Chem. Soc. 125 (2003) 15651–15658.
[39] D. Sajan, H. Joe, V.S. Jayakumar, J. Zaleski, J. Mol. Struct. 785 (2006) 43–53.
[40] L.S. Pu, ACS Symp. Ser. 455 (1991) 331–342.
[41] K.S. Thanthiriwatte, K.M. Nalin de Silva, J. Mol. Struct. (Theochem.) 617 (2002) 169–175.
[42] R.G. Pearson, Proc. Natl. Acad. Sci. 83 (1986) 8440–8441.